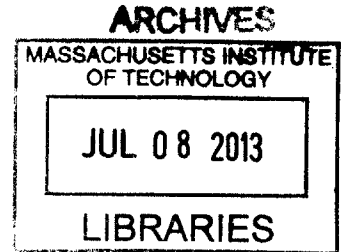# Iron (III) Chloride Doping of Large-Area Chemical Vapor Deposition Graphene
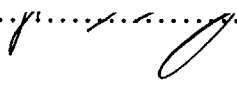
By

Yi Song
B.S. Electrical Engineering
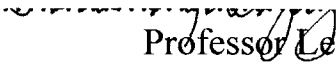University of California, Berkeley 2011

SUBMITTED TO THE DEPARTMENT OF
ELECTRICAL ENGINEERING AND COMPUTER SCIENCE
IN PARTIAL FULFILLMENT OF THE REQUIREMENTS FOR THE DEGREE OF
MASTER OF SCIENCE IN ELECTRICAL ENGINEERING
AT THE
MASSACHUSETTS INSTITUTE OF TECHNOLOGY
JUNE 2013

Author: ....
Department of Electrical Engineering
May 21, 2013

Certified by: ....
Professor Jing Kong
Associate Professor of Electrical Engineering
Thesis Supervisor

Accepted by: ....
Professor Leslie A. Kolodziejski
Graduate Officer, Professor of Electrical Engineering

Iron (III) Chloride Doping of Large-Area Chemical Vapor Deposition Graphene

By

Yi Song

Abstract

Chemical doping is an effective method of reducing the sheet resistance of graphene. This thesis aims to develop an effective method of doping large area Chemical Vapor Deposition (CVD) graphene using Iron (III) Chloride ($FeCl_3$). It is shown that evaporating $FeCl_3$ can increase the carrier concentration of monolayer graphene to greater than $7x10^{13}cm^{-2}$ and achieve resistances as low $72\Omega/sq$. We also evaluate other important properties of the doped graphene such as surface cleanliness, air stability, and solvent stability. Furthermore, we compare $FeCl_3$ to three other common dopants: Gold (III) Chloride ($AuCl_3$), Nitric Acid (HNO_3), and TFSA (($CF_3SO_2)_2NH$). We show that compared to these dopants, $FeCl_3$ can not only achieve better sheet resistance but also has other key advantages including better solvent stability and better heat stability.

Thesis Supervisor: Jing Kong

Title: Associate Professor of Electrical Engineering

4

Contents

List of Figures

List of Tables

Chapter 1

1 Introduction

1.1 Background in Graphene Doping

Because of its high electrical conductance, high optical transmittance and excellent flexibility, graphene has attracted much attention in the field of flexible optoelectronics. Chemical Vapor Deposition (CVD) growth on copper allows for mass production of large area monolayer graphene suitable for electrodes in optoelectronic devices [1]. However, monolayer graphene typically has sheet resistance of several hundred ohms, which is significantly higher than that of Indium Tin Oxide (ITO), which is the industry standard[2]. This can introduce a significant series resistance in solar cells or LEDs and will inevitably degrade device performances. Stacking multiple layers of graphene does improve the overall resistance at the expense of optical transmittance[3, 4]. Even with multiple layers, however, the I-V curves of CVD graphene-based devices show significant series resistances and the efficiency of these devices remain inferior to that of their ITO-based counterparts[3]. Furthermore, the process of transferring graphene layer-by-layer is time consuming and the resistance does not always scale linearly with the number of layers[5, 6].

Another common method to improve the resistance of graphene electrodes is chemical doping. P-type dopants can substantially improve the conductivity of graphene with little impact in optical transmittance. Currently, the most commonly-used dopants are Gold Chloride ($AuCl_3$) and Nitric Acid (HNO_3). Kim et al. demonstrated that $AuCl_3$ can reduce the resistance of monolayer graphene by up to 77% to 150Ω/sq [7]. Bae et al. reported similar results using HNO_3, reducing the resistance by 60% to 125Ω/sq [6]. However, both types of doping are unstable in air; the sheet resistance increases quickly over the first few days and eventually saturates at roughly 200% of the resistance immediately after doping[8, 9]. Furthermore, AuCl3 leaves gold particles up to 100nm in diameter on the surface of the graphene, which can cause shorts in thin-film vertical devices [7]. Other dopants include bis(trifluoromethanesulfonyl)amide (TFSA), which was used to achieve 8.6% efficiency in graphene/n-Si Schottky solar cells, and tetracyanoquinodimethane (TCNQ), which his compatible with layer-by-layer graphene transfer. Both of these also have disadvantages, as TCNQ requires a lengthy evaporation process and TFSA – though stable in air – also leaves residues and dissolves in common solvents such as Isopropanol. An ideal dopant for CVD graphene will have the following characteristics:

1. Can achieve low sheet resistance
2. Stable in atmosphere
3. Stable in solvents (water, IPA, Acetone, etc)
4. Clean
5. Fast
6. Economic
7. Compatible with multi-layer transfer

9

Unfortunately, it is highly unlikely that any dopant can exhibit all of these characteristics so the most appropriate one must be selected based on the particular application.

In 2012, Khrapach et al. demonstrated that intercalation doping on exfoliated graphene using Iron (III) Chloride (FeCl₃) can achieve resistances as low as 8.8Ω/sq at 84% transmittance with 5-layer graphene [10]. Furthermore, this type of doping is stable in air for up to one year. However, HOPG graphene cannot be mass-produced and therefore cannot be used for large-area practical optoelectronic devices. To make matters worse, the doping process entails pumping a sealed chamber down to 2×10^4mbar, which requires a turbo pump and, and the intercalation process takes 10h. Nonetheless, this work highlights the advantages of FeCl₃ doping over other methods and may be promising if applied to CVD graphene.

1.2 Scope of This Work

The goal of this thesis is to twofold: first, we refine the process of FeCl₃ doping for CVD graphene characterize the results. Next, we compare the effectiveness of FeCl₃ to other dopants based on the aforementioned metrics. Chapter 2 offers an overview of graphene, in particular, its synthesis and transfer and how these processes affect the sheet resistance. Chapter 3 discusses the doping procedure itself, including what works and what does not work, and evaluates characteristics of FeCl₃-doped graphene. Chapter 4 brings into the discussion three additional dopants: Gold(III) Chloride (AuCl₃), Nitric Acid (HNO₃), and TFSA. FeCl₃ is compared to these dopants in terms of the important metrics and it is shown that FeCl₃ has some key advantages and disadvantages. Chapter 5 provides a summary of our findings and some additional discussion.

Chapter 2

2 Background in Graphene

2.1 Sheet Resistance Considerations

The sheet resistance of graphene is determined by two parameters: carrier mobility (μ), measured in cm^2/Vs and sheet carrier concentration (n), measured in cm^{-2}. These parameters are related to the sheet resistance by the following expression.

$$R_{sh} = \frac{1}{q\mu n} \qquad (1)$$

Theoretical calculations suggest that in intrinsic graphene, the mobility at carrier density of $10^{12}cm^{-2}$ is as high as 200 000cm^2/Vs at room temperature, which yields sheet resistance of 30Ohms[11]. This is equivalent to 10^8S/m in three-dimensional conductivity, which is superior to that of aluminum or copper. However, the 30Ohms result assumes flat, suspended, single-crystalline graphene in vacuum, in which case only electron-phonon scattering contributes to resistance. In practice, numerous additional sources of scattering such as wrinkles, domain boundaries, substrate interactions, and charged impurities make it difficult to achieve this 200000cm^2/Vs figure, especially for large area CVD graphene.

Thus, an alternative strategy for lowering the resistance of graphene is to dope it as heavily as possible. It is clear from the above expression that in order to minimize resistance, we should maximize both mobility and carrier concentration. However, increasing carrier concentration via doping inevitably increases charge impurity scattering, thus degrading mobility according to the Drude model. In fact, if the carrier concentration is high enough, charged impurity scattering becomes the dominant scattering source and other sources such as substrate interactions no longer matter. However, it is possible for the doping process to introduce defects in the graphene, which further reduces effective mobility. Thus, the goal of doping should be to increase carrier concentration as much as possible while minimizing the decrease in mobility.

The sheet resistance can be measured using Van der Pauw's method, which entails I/V measurements from a series of four contacts placed on the periphery of the sample. The carrier concentration can be determined using four probe Hall measurements. The mobility of the sample can be derived from the results of the two measurements. In this work, all sheet resistance and carrier concentration measurements are performed using a home-built four-point-probe station and a 2000Gs permanent magnet.

11

2.2 Synthesis and Transfer

Although the synthesis and transfer of CVD graphene is not the focus of this work, it is quite a sensitive process with details pertinent to doping.

2.2.1 Growth

The graphene used in this work is synthesized using Low-Pressure Chemical Vapor Deposition (LPCVD) on copper foil[12]. The schematic of the system is shown in Figure 2-1. Growth on copper foil produces a uniform monolayer, as opposed to growing on nickel, which produces non-uniform multilayer graphene[13]. Before growth, the copper foil was cleaned by sonicating in nickel etchant (type TBP) for 30s and rinsing with DI water. After cleaning, the copper foil was placed in a quartz tube and annealed at 1000°C for 30min while flowing 10sccm H_2. Graphene was then grown for 30min by increasing H_2 flow rate to 70sccm and setting the CH_4 flow rate 0.5sccm. The chamber pressure was 400mTorr during the annealing phase and 1.90Torr during the growth phase. The influence of growth variables such as gas flow rates, partial pressures, and temperature on the quality of graphene is beyond the scope of this work. However, from our experiences, the resistance of the graphene film is not strongly dependent on growth conditions, with 0.5sccm CH_4 and 70sccm H_2 producing similar results as 20sccm CH_4 and 10sccm H_2.
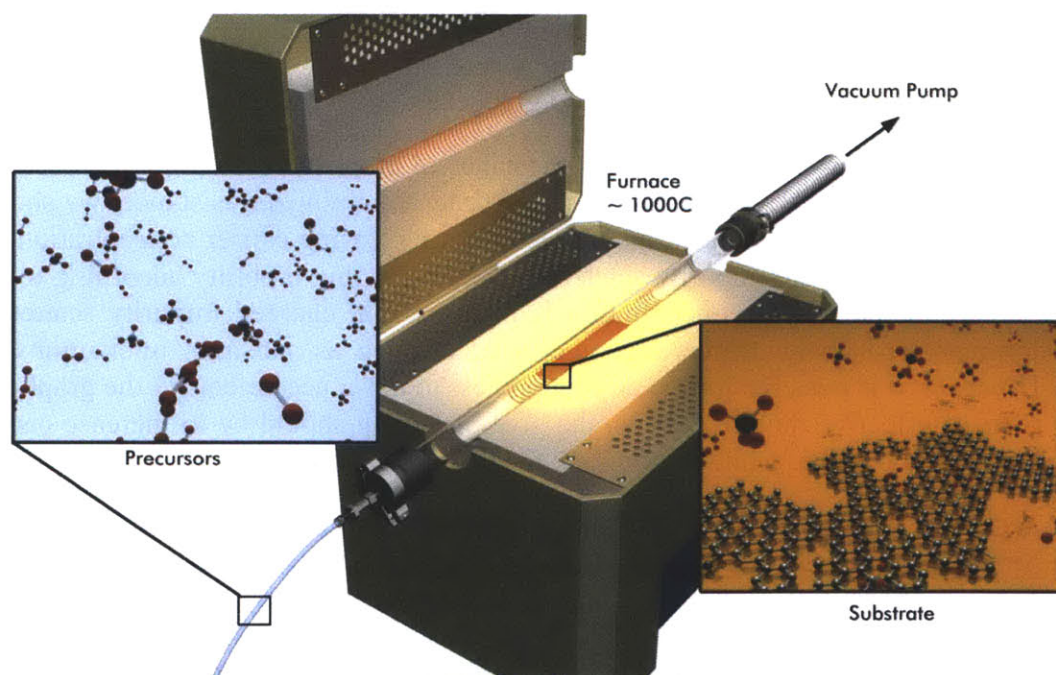

Figure 2-1. System used for synthesis of CVD graphene on copper foil. Components are roughly to scale.

2.2.2 Transfer

PMMA (950k 4.5% dissolved in Anisole) is spin-cast at 2500rpm onto the graphene/copper, producing a 300nm film. If a very clean surface is needed, the graphene on the back side can be removed using O_2 plasma. The stack is then placed PMMA-side-up in CE-100 copper etchant (mixture of HCl and $FeCl_3$) for 15min, allowing the copper to completely dissolve. The PMMA/graphene film remains floating and is transferred into 10% HCl using a glass slide for 20min to remove $FeCl_3$ residues. Finally, the film is rinsed with DI water for some amount of time (discussed later) and fished onto the target substrate, typically 300nm SiO_2. The process is illustrated in Figure 2-2.
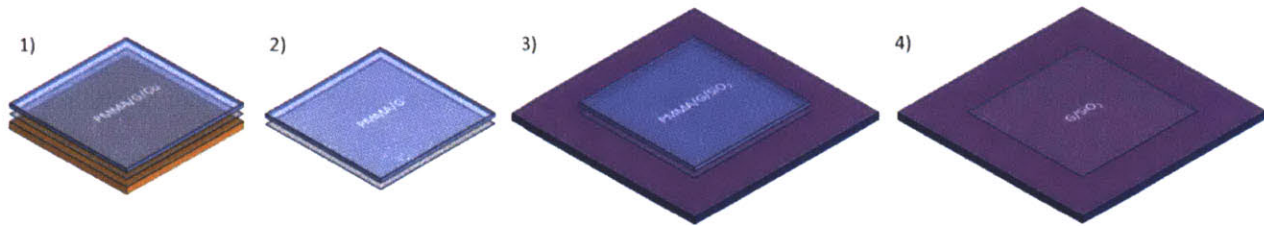
Figure 2-2. Transfer of graphene onto SiO_2 using PMMA as an intermediate membrane.

2.2.3 PMMA Removal

The complete removal of PMMA residues can be challenging. Currently, the most popular options are dissolving in acetone or thermal annealing, or some combination of the two.

There are numerous variations for removing PMMA with acetone. Immersing at room temperature for several minutes, immersing overnight, immersing in heated acetone, heated acetone vapor, and sonication in acetone are all valid options and our experiences suggest that there is little difference between them. However, it is critically important that there is no water residue between the graphene and substrate prior to acetone treatment, or the graphene will tear during the process. To ensure this, we first place the substrate/graphene/PMMA stack in an oven set to $80^{\circ}C$ for 5min to evaporate most of the trapped water and then bake the sample for 20min at $130^{\circ}C$ to remove any remaining residues. Using this procedure, we find that sample is sufficiently rid of water that dissolution is acetone does minimal damage to the graphene. After acetone treatment, the graphene sample typically has mobility of $3500cm^2/Vs$ with carrier concentration of $3\times10^{12}cm^{-2}$ for ~600Ohm/sq sheet resistance. Rinsing the graphene in DI water for longer periods of time before transferring onto the target substrate results in lower carrier concentration (~$2\times10^{12}cm^{-2}$ if left in DI water overnight) and higher mobility (~$4000cm^2/Vs$). However, the decrease in carrier concentration is greater than the increase in mobility so the sheet resistance increases slightly. Leaving the sample in air causes light p-doping; after one week, the carrier concentration typically increases to $5\times10^{12}cm^{-2}$ and the sheet resistance decreases to ~500Ohm/sq.

A second option of PMMA removal is thermal annealing; the graphene is placed in an Argon/Hydrogen environment and heated to $300-500^{\circ}C$ for 2-3h. This is done to completely

remove PMMA residues, leaving a clean surface for further processing[2, 14]. Typically, this step is added after acetone treatment but can be performed directly after transfer at the expense of leaving more PMMA residues[2]. However, the high temperature causes the graphene to conform more closely to the underlying SiO_2, which results in hole doping and degraded mobility[15]. In some cases, the hit on electrical performance is undesirable but in the case of conducting electrodes, the increase in carrier concentration outweighs the reduction in mobility, resulting in an overall decrease in sheet resistance. Typical values after annealing are $2000cm^2/Vs$ mobility and $1\times10^{13}cm^{-2}$ carrier concentration for ~300Ohm sheet resistance. It is worth noting, however, that the extra scattering term associated with increased surface roughness also affects carriers introduced via chemical doping. In other words, we expect that a chemically doped, annealed sample would have worse mobility than a similarly doped sample that has only received acetone treatment. However, as previously mentioned, for chemically doped samples, the dominant scattering mechanism is charge impurity scattering, so it is uncertain whether roughness scattering plays a key role in determining the final sheet resistance. We briefly investigate this effect in this work.

There exists other for removing PMMA residues. Scanning the graphene surface with an atomic force microscope (AFM) tip also cleans it, but this method is obviously impractical for large areas[16, 17]. Chloroform and formamide have been shown to lower the intrinsic doping level better than acetone[15, 18]. From our experiences, nitromethane is also more effective than acetone in removing PMMA, but it is not clear if nitromethane immersion has any unwanted side effects. Thus, to minimize the number of unknowns, we only consider acetone treatment and annealing.

Chapter 3

3 Doping CVD Graphene with FeCl3

3.1 Procedure

3.1.1 Initial Tests

The graphene (on SiO_2) and $FeCl_3$ (anhydrous 98% acquired from Alfa Aesar) were placed in a glass pipette and pumped down using a dry scroll pump. Because of equipment limitations, the minimum pressure achieved was 40mTorr. After base pressure is reached, a blow torch is used to seal the pipette. After giving the pipette sufficient time to cool, the graphene sample was slid in the pipette to a position ~10cm from the $FeCl_3$. The pipette was then placed in a tube oven heated to 360°C with the graphene sample in the middle and the $FeCl_3$ at the periphery, as shown in Figure 3-1. The temperature at the $FeCl_3$ location was measured to be 320°C. After 10h, the pipette was broken and the sample was removed.
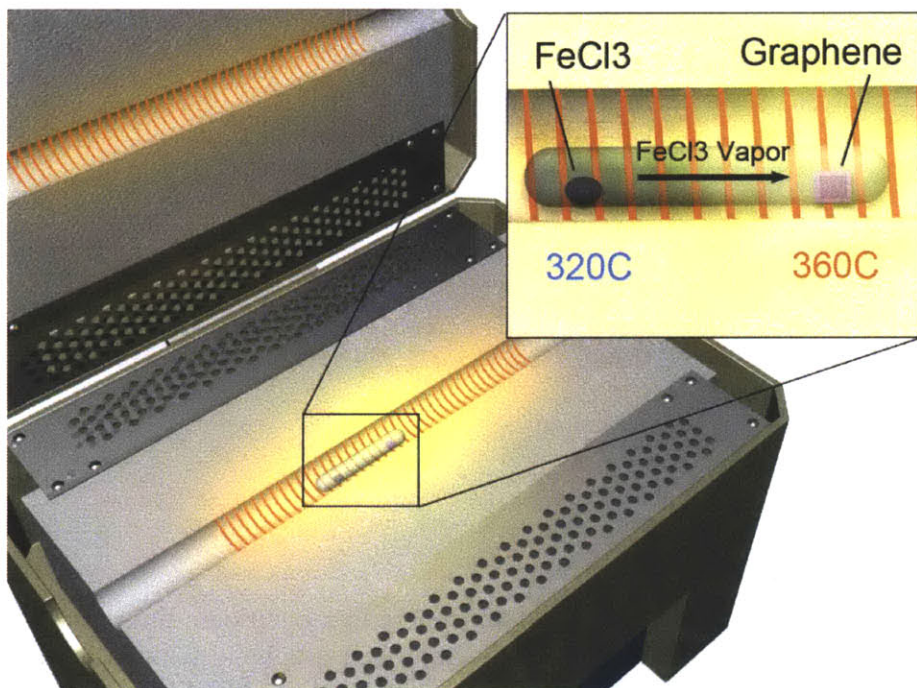
Figure 3-1. Basic system for $FeCl_3$ doping. Components are drawn roughly to scale.

For all doping attempts using the conditions outlined above, upon breaking the pipette, we find that the graphene is completely broken. Thus, the parameters used by Krapach et al. for exfoliated graphene does not appear to work for CVD graphene. Exposing CVD graphene to $FeCl_3$ at 360°C for longer periods of time under vacuum causes the graphene to break and crumple on the substrate; this occurs regardless of whether the graphene was annealed or not. This result is not surprising because CVD graphene is inherently polycrystalline, which allows

for $FeCl_3$ to penetrate underneath through the domain boundaries and strip the graphene from the substrate. As shown in Figure 3-2, lowering the temperature to $320^{\circ}C$ or $280^{\circ}C$ does help but even at these lower temperatures, the graphene is still broken.
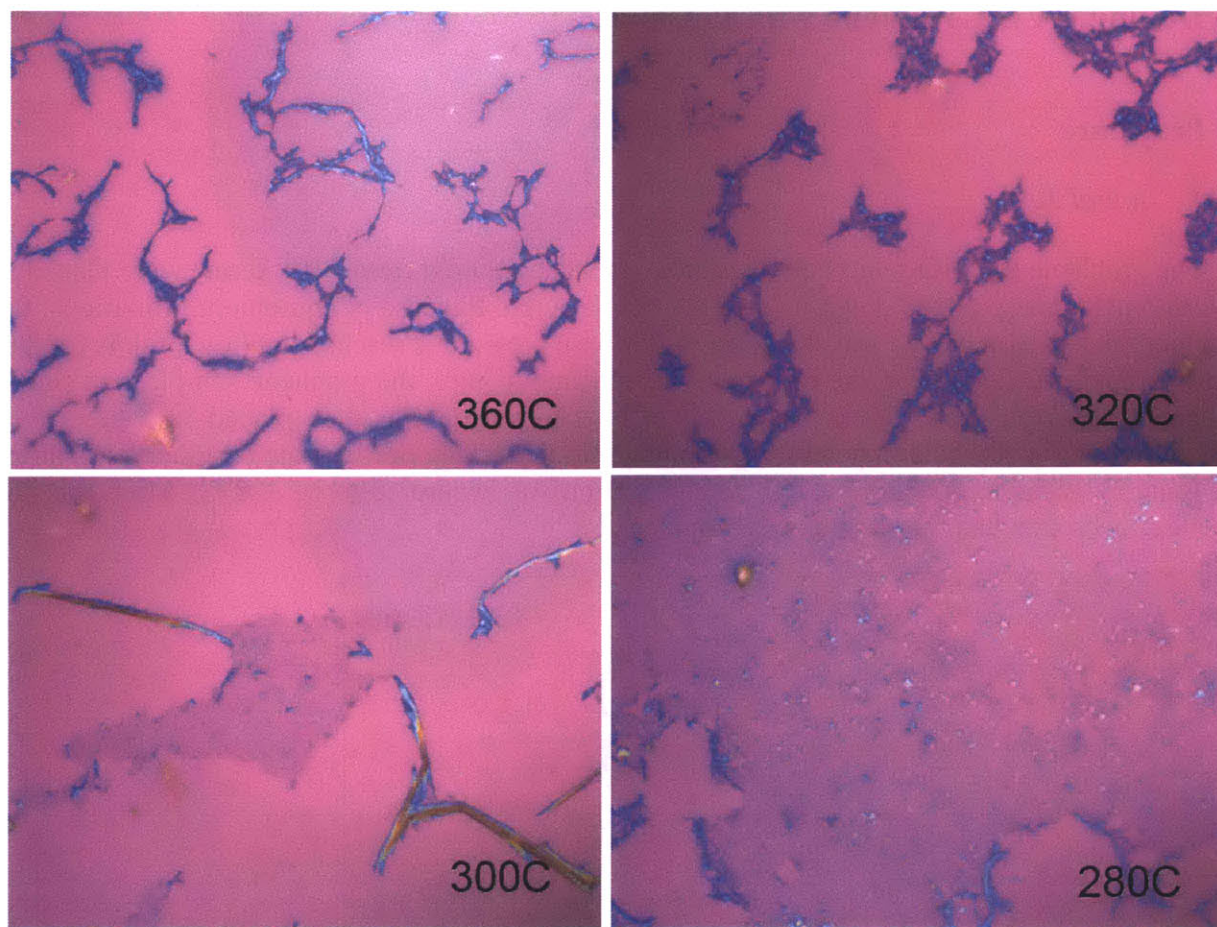
Figure 3-2. Graphene after 1h in $FeCl_3$ vapor at high temperatures.

3.1.2 Optimized Procedure

After a trial-and-error process, we find that doping in atmosphere in the temperature range of $320^{\circ}C$ - $360^{\circ}C$ for a short amount of time (1-5min) produces unbroken graphene with excellent sheet resistance (~100Ohm/sq). Lower temperatures for longer times, such as $240^{\circ}C$ for 1h, also strongly dopes the graphene, but tends to leaves more residues, presumably due to the longer amount of time the graphene is left in the vessel.

Ambient pressure is selected over low pressure because the $FeCl_3$ evaporates more quickly under vacuum, making the reaction more difficult to control. Furthermore, sealing under ambient pressure does not require a vacuum pump, making the process more economic. From our experiences, heating graphene to $360^{\circ}C$ in atmosphere for longer times (1 hour) severely

16

degrades mobility but shorter times have little effect. It is also important that the pipette is broken immediately after removing from the oven, as the $FeCl_3$ vapor will condense on the surface of the graphene if given time to cool, as shown in Figure 3-3. The condition used for the remainder of this manuscript, unless otherwise mentioned, is 360°C for 90s.
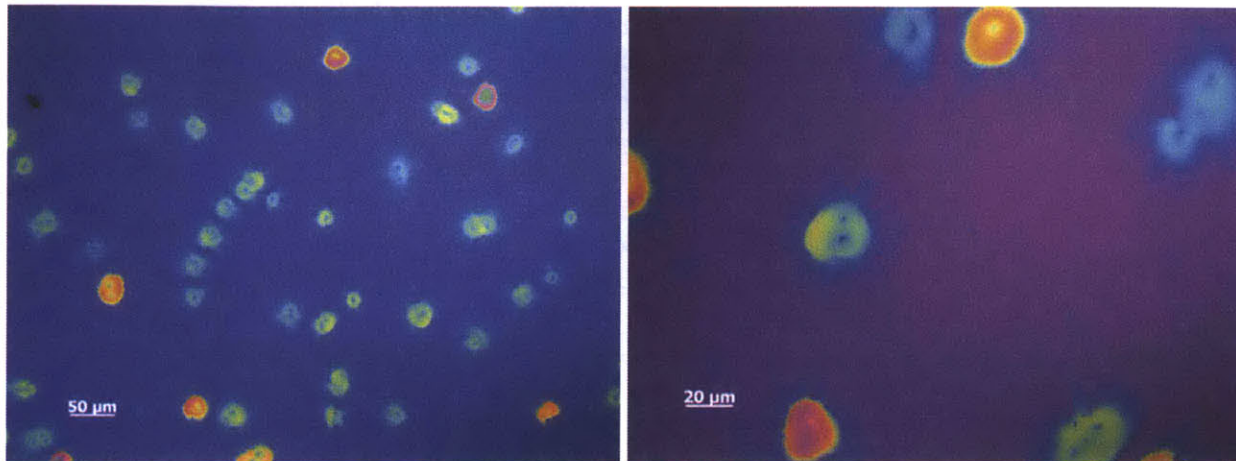
Figure 3-3. $FeCl_3$ condensed on graphene surface.

3.1.3 Other Modifications and Considerations

We also tried filling the pipette with argon before sealing, but the effect does not appear to be any different from heating in air. Changing the relative positions of the $FeCl_3$ and the sample, for example, placing the $FeCl_3$ in the middle of the furnace, also does not appear to have any significant effect on the outcome. Placing the sample face-down in the pipette causes more residues to build up on the surface; it is unclear to us why this happens. If the sample inverts during the procedure or quickly slides from the hotter end of the pipette to the cooler end, residues will also build up on the surface. Thus, care must be taken when removing the pipette from the furnace. In spite of the many subtleties highlighted above, we were able to obtain clean samples with reasonable consistency after some refinement in handling technique.

The size of the pipette limits the size of the sample to approximately 2x4mm, which is still large enough to place indium contacts by hand. We test the same procedure for a larger sample (1cmx1cm) sealed in a test tube. Similar results are achieved with a slight increase in heating time to 120s in order to compensate for the larger system.

To make $FeCl_3$ doping more practical for mass-production, we built a modified system illustrated in Figure 3-4. The samples are placed on a quartz boat at the center of a 1-inch quartz tube and $FeCl_3$ is placed in a crucible approximately 5cm from the samples. The tube is heated to 360°C, as before, allowing the $FeCl_3$ to evaporate. There is nothing constraining the $FeCl_3$ vapor to the region with the samples; if left long enough, the vapor will diffuse to the colder regions closer to the edges of the tubes. However, we find that the vapor stays in the middle for approximately 10min, which is long enough to dope the samples.

17
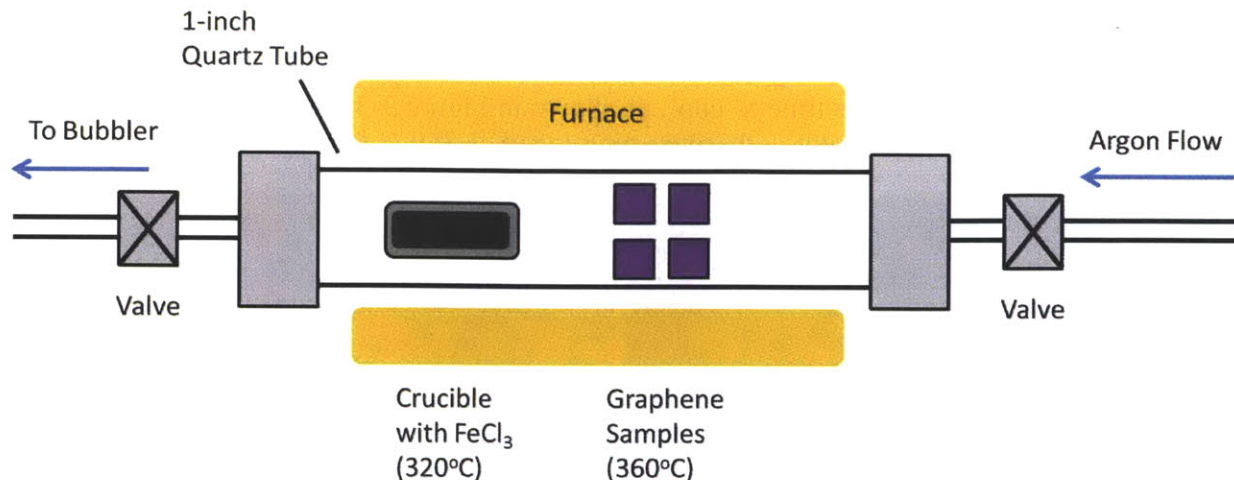
Figure 3-4. Schematic of mass production doping system. Drawing not to scale.

Because the system is much larger than a pipette, the $FeCl_3$ vapor is not as dense and therefore, the samples produced using this setup were slightly less doped. The average sheet resistance was 109Ohms, with most samples ranging from 100 to 120Ohms. The consistency of sheet resistance within a single run was quite good; a batch six samples doped simultaneously had sheet resistance of 105±5Ohms. This system proved to be quite effective at doping many samples at once, but the overhead time for setting up and position all components makes it less practical for small-scale experiments. Thus, for the remainder of this thesis, the samples mentioned are all doped using the pipette.

3.2 Characterization of FeCl₃ Doped Graphene

3.2.1 Sheet Resistance and Carrier Concentration

$FeCl_3$ doping can produce monolayer graphene with lower sheet resistance than other doping methods. The best sample was measured to be 72 Ohms per square, which is currently the lowest value reported in literature. Most samples are doped to roughly $5 \times 10^3 cm^{-2}$ with sheet resistance between 85 and 100 Ohms; the slightly worse samples are in the range of 110-120Ohm. The average carrier concentration was $5.0 \times 10^3 cm^{-2}$ (3-6) and the average sheet resistance was 94 Ohms per square (3-5), which is, again, the best value reported in literature so far.

18

FeCl3 Doping Sheet Resistance Distribution
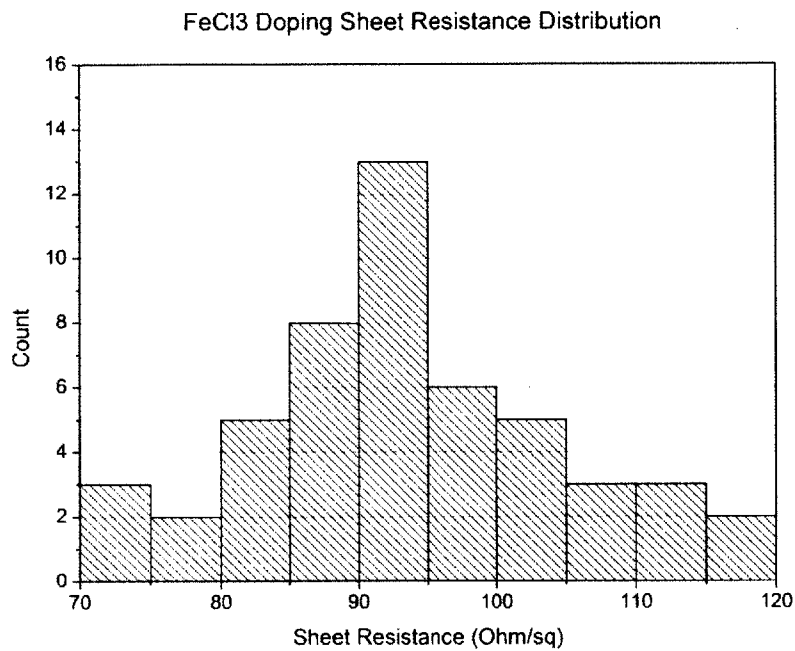
Figure 3-5. Histogram of the sheet resistance of $FeCl_3$-doped graphene.

FeCl3 Doping Carrier Concentration Distribution
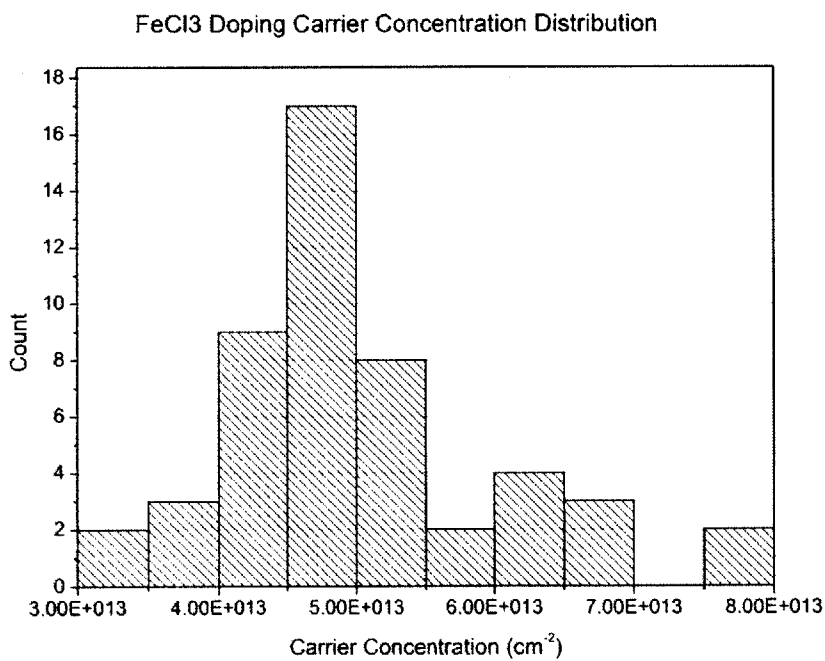
Figure 3-6. Histogram of the carrier concentration of FeCl3-doped graphene.

One peculiarity is that the final mobility and carrier concentration values after doping do not depend on whether the PMMA was removed using acetone or annealing. The decrease in

19

mobility associated with annealing becomes apparent at annealing temperatures as low as 300°C, which may imply that FeCl$_3$ doping conditions, in effect, anneal the sample. To test this hypothesis, we expose acetone treated samples to 360°C in ambient – without FeCl$_3$ – for 2min. However, the samples subjected to this test do not exhibit reduced mobility, which suggests that 2min at 360°C is insufficient for annealing. Thus, we conclude that the scattering from heavy doping or surface residues is dominant over roughness scattering caused by annealing. This observation can be considered an advantage because it would allow for heavy doping on substrates that cannot survive high annealing temperatures.

3.2.2 Surface Cleanliness

In general, the doped graphene looks clean optically as shown in Figure 3-7, the residues are visible under SEM (Figure 3-8 a,b) and AFM. In roughly 20% of attempts, even using the optimized doping conditions, the graphene turns out dirty (Figure 3-8 c,d).
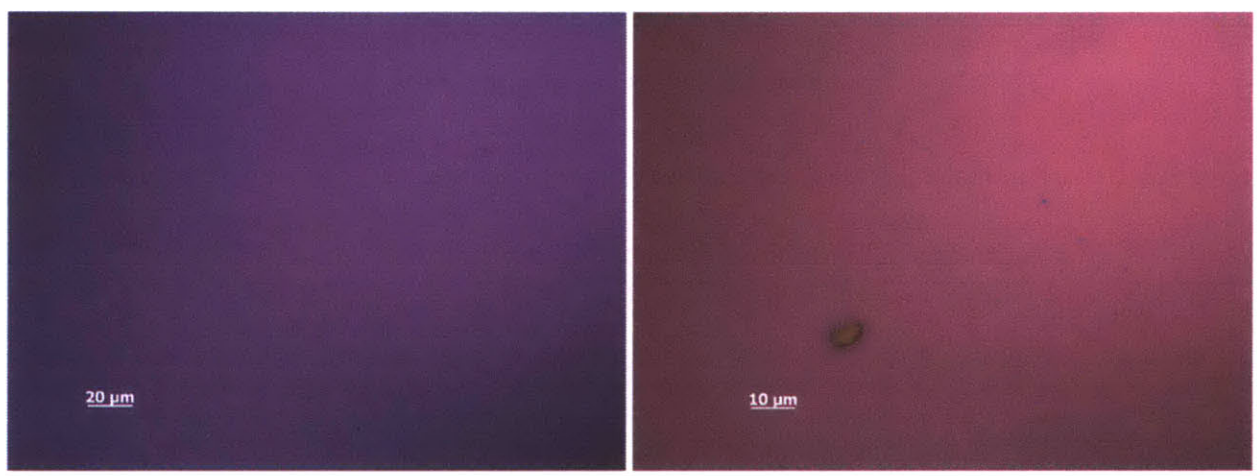
Figure 3-7. Graphene cleanly doped with FeCl$_3$.
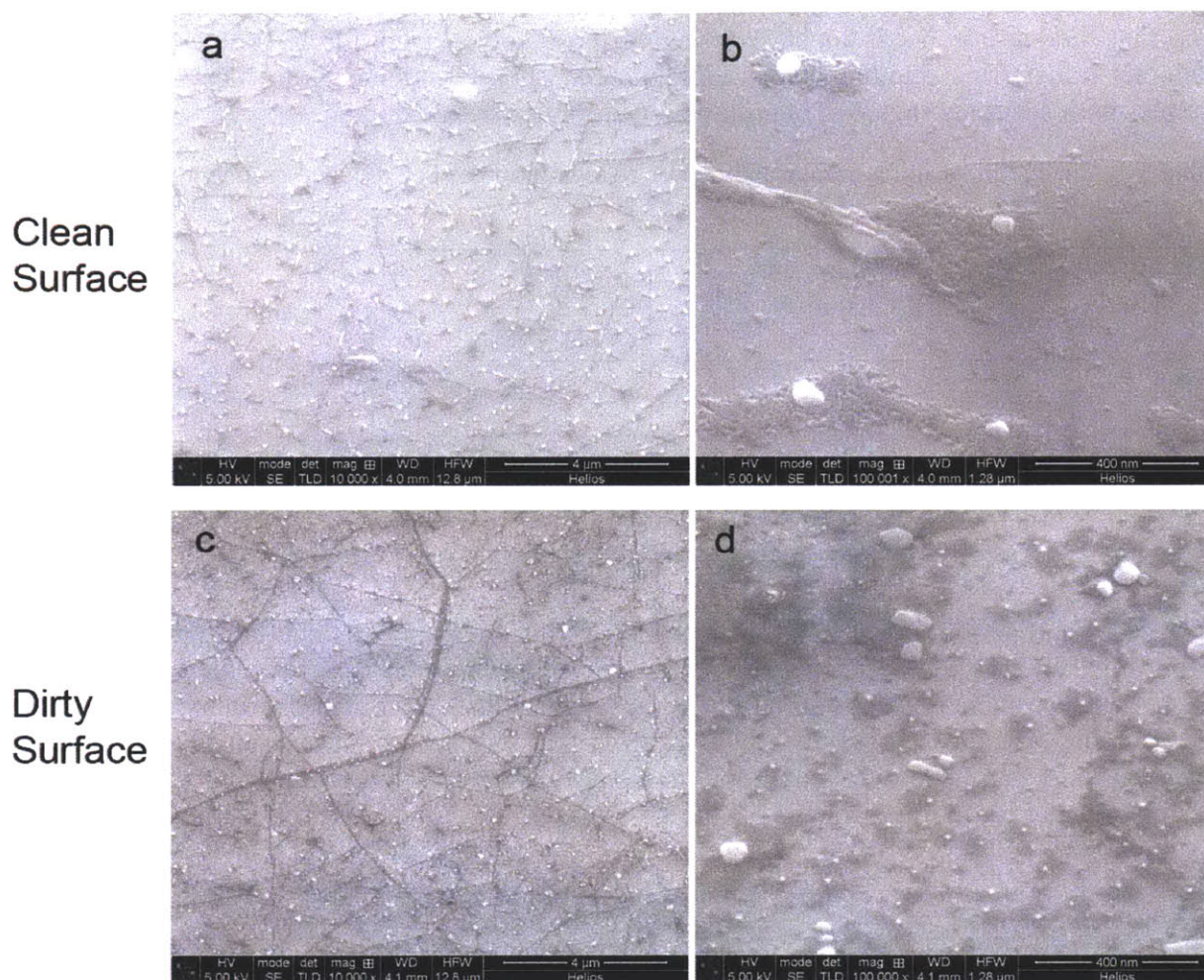
Figure 3-8. a,b) SEM of an FeCl₃ doped graphene sample that looks clean under optical microscope. c,d) Sample that looks dirty visually.

Particles on the surface are almost always undesirable, as they can reduce optical transmittance as well as make it difficult to do fabrication on the sample. Unfortunately, charge transfer doping, by definition, requires the presence of particles on the surface. It may be possible to limit the formation of particles by heating the substrate to a higher temperature than the surroundings to prevent condensation but this is not possible using our apparatus. Developing a system that improves surface cleanliness will be a subject of future investigations.

3.2.3 Stability in Solvents

For photovoltaic applications, graphene is typically subjected to several fabrication steps after transfer, some of which may involve spin-casting organics. Thus, it can be important that the dopant is able to resist standard solvents such as water, acetone, isopropanol (IPA),

nitromethane, and anisole. We immerse doped samples in these standard solvents for 120s to evaluate the stability of $FeCl_3$. 2 minutes is chosen because it reflects the approximate amount of time that the sample needs to be exposed to these solvents for further processing steps (for example, transferring another layer of graphene). The measurements are done with annealed samples with sheet resistance of approximately 30Ohm before doping.

Table 3-1. Change in sheet resistance and carrier concentration of $FeCl_3$ doped graphene after immersion in various solvents.

Solvent	% Change in Resistance	% Change in Carrier Concentration
Water	+182 %	-36 %
IPA	+6 %	-7 %
Acetone	+63 %	-38 %
Nitromethane	+50 %	-42 %
Anisole	+3 %	-7 %

As the chart above shows, $FeCl_3$ resists IPA and anisole quite well but does not resist acetone or nitromethane. In the case of water, the carrier concentration decreases moderately but the sheet resistance increases substantially, which suggests that water immerse damages the sample and degrades mobility. The author hypothesizes that this occurs because the $FeCl_3$ permeates underneath the graphene, weakening the graphene-substrate adhesion, allowing the high surface tension of water to rip the graphene off the substrate.

3.2.4   Stability in Air

It has been reported in literature that HNO_3 and $AuCl_3$ are very unstable in atmosphere and the sheet resistance eventually settles to 200% its original value. TFSA, owing to its hydrophobicity, is air stable. Figure 3-9 shows the time evolution of sheet resistance and carrier concentration after $FeCl_3$ doping. The resistance increases by roughly 80% over the course of several weeks, mostly owing to a 50% drop in carrier concentration. However, because the dopant is stable in anisole, coating the samples with a protective layer of PMMA prevents the degradation in sheet resistance. Using a PMMA coating, the sheet resistance increases by only 4% over 3 weeks.

FeCl3 Electrical Properties Over Time
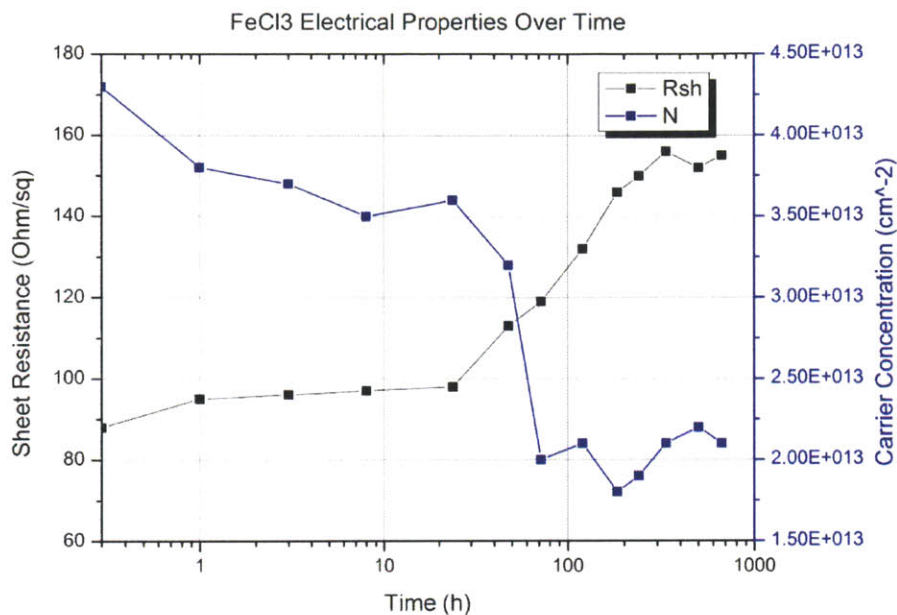
Figure 3-9. Time evolution of the electrical properties of FeCl$_3$ doped graphene. The data is averaged over three samples.

We also consider the effects of higher temperatures on the change in sheet resistance over time. We suspect that the dopant molecules on the surface of the samples degas over time and higher temperatures will likely speed up the process. Because some processing such as evaporation and baking requires higher temperatures, most likely in the 80°C-250°C range, it is important to observe whether FeCl$_3$ can retain low sheet resistance at these temperatures.

Sheet Resistance at Higher Temperatures Over Time
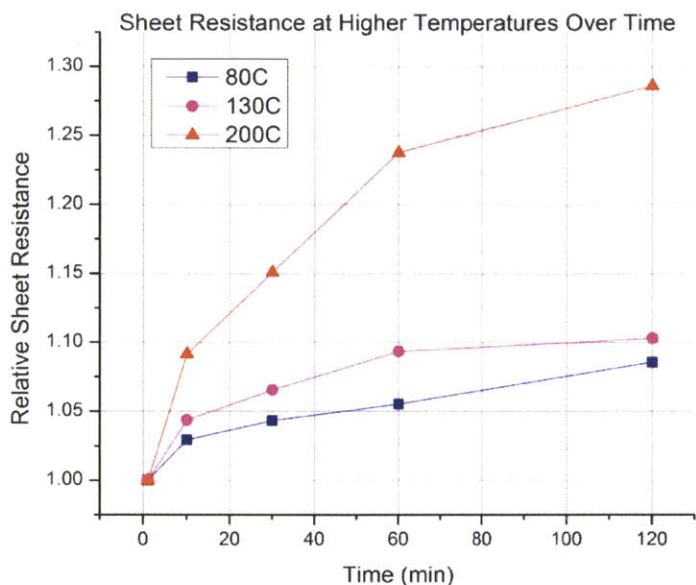
Figure 3-10. Change in sheet resistance of $FeCl_3$ doped graphene over time at higher temperatures.

The experiment was done over a timeframe (120min) that reasonably reflects the amount of time needed for additional processing steps. Because the sheet resistance increases rapidly immediately after doping in atmosphere even at room temperature, we wait 24h after doping before subjecting the samples to the higher temperatures. It appears that the graphene doping is reasonably stable at temperatures up to $130^{\circ}C$ but becomes much less stable at $200^{\circ}C$, with sheet resistance increasing by 28% over 2h.

3.2.5   Effectiveness in Multi-layer Samples

Krapach reported that the sheet resistance of $FeCl_3$-doped exfoliated graphene decreases significantly with layer number. This is likely due to the fact that the $FeCl_3$ intercalates between the graphene layers, which reduces interlayer coupling. The result is a series of independently-conducting doped graphene layers, which, as expected, become more conductive as the number of layers increase.

Multi-layer CVD graphene is inherently different from multi-layer exfoliated graphene because the layers are transferred independently and conduct current independently. Typically, this multi-layer configuration is referred to as "stacked multi-layer," to distinguish between multiple transfers and true multi-layer CVD graphene grown, say, on Ni foil[5]. Because $FeCl_3$ is soluble in water, it is not possible to transfer multiple layers and dope each layer separately, as it is with TCNQ[19]. Thus, we test the effectiveness of $FeCl_3$ in doping multi-layer samples by transferring all layers first and evaporating onto the entire stack. Multilayer graphene is more resistance to damage from the $FeCl_3$, which allows us to dope for longer time. Accordingly, the 2-layer samples were doped for 120s while the 3 and 4-layer samples were doped for 180s.

24

Doping for longer than 180s causes residues to start forming on the surface. We acknowledge that the improvement in sheet resistance for multilayer samples may be attributed to the longer time, but it makes sense to compare the best condition given the number of layers. The average sheet resistance versus number of layers is shown in Figure 3-11.
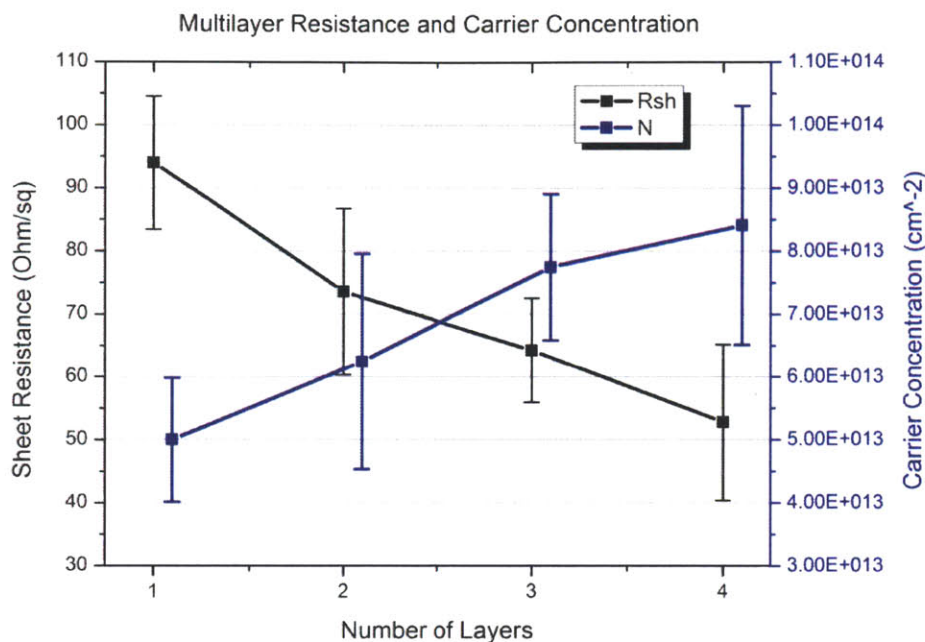
Figure 3-11. Sheet resistance and carrier concentration for multilayer $FeCl_3$ doped graphene samples.

Judging from the plot of average carrier concentration versus number of layer, it appears that, at least to some extent, $FeCl_3$ can penetrate into the lower layers. However, the resistance still does not fall off proportionally to layer number, which suggests that some layers (most likely bottom ones) are not doped as heavily as others. Other transfer techniques[20] that do not require water immersion may be compatible with layer-by-layer doping using $FeCl_3$ but consistently applying these techniques to large areas has been challenging. The best 4-layer sample was measured to be 41Ohm/sq.

3.2.6 Raman Signature

Resonant Raman Spectroscopy is a commonly-used tool for evaluating the quality of graphene[21]. The Raman spectrum of pristine graphene has two distinct features: the "G-peak" at roughly 1580cm^{-1} and the "G'-peak" at 2700cm^{-1}. Figure 3-12 shows the Raman spectrum of $FeCl_3$-doped graphene compared to that of pristine CVD graphene with their respective G-peak positions.
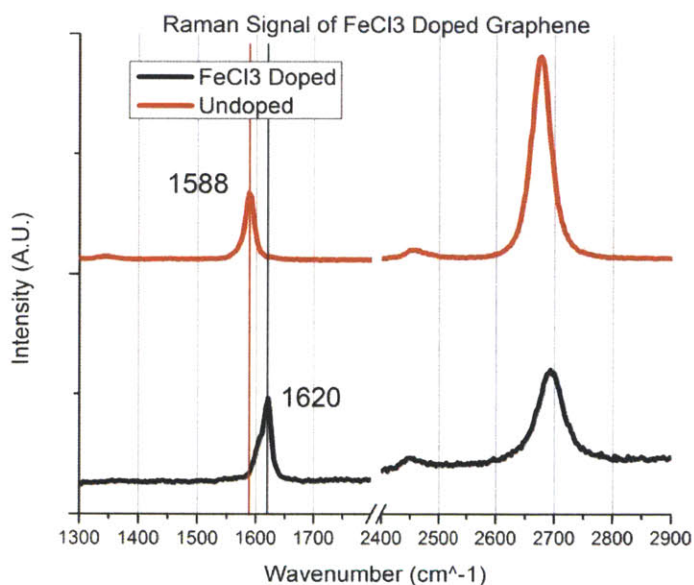
Figure 3-12. Raman spectrum of FeCl$_3$-doped graphene compared to pristine graphene.

The physics behind Raman is beyond the scope of this work, but we address the origins of several key features. It has been reported literature that hole doping causes the G-peak to blue-shift[15, 22, 23]. From the data acquired by Das et al. a shift to 1620cm^{-1} represents extremely heavy hole-doping in excess of $3x10^{13}cm^{-2}$, which is consistent with our electrical measurements. The peak position is slightly higher than the figure of 1612cm^{-1} reported by Krapach et al. for graphene with one adjacent FeCl$_3$ layer. The same report also demonstrates that the relative intensity of the G'-peak decreases as doping increasing, which is also consistent with our observations. Our Raman spectrum is also consistent with that reported by Zhao et al. for few-layer graphite flakes intercalated with FeCl$_3$[24]. Finally, we note that the "D-band", which occurs at 1365cm^{-1} and is normally associated with defects in graphene is not present in either case. This suggests that FeCl$_3$ does not significantly damage the graphene.

Chapter 4

4 Comparison of Doping Methods

4.1 Common Dopants

The additional dopants discussed in this work are Gold (III) Chloride, Nitric Acid, and TFSA. All of these dopants have history rooted in efforts to dope carbon nanotubes. Because of their similar atomic structure, it is of little surprise that the same dopants are effective for graphene. $AuCl_3$ and HNO_3 have been reported extensively in literature. TFSA is a more recent development, best known for its stability in air and for its use in achieving 8.6% efficient graphene-silicon Schottky solar cells[25, 26]. Other types of dopants such as $SOCl_2$[27] and TCNQ[19] have also been reported, but from literature reports and our own experiences, these dopants are not very effective (not significantly increasing carrier concentration beyond that of annealed samples). Values reported in literature are shown in Table 4-1. We choose $AuCl_3$, HNO_3, and TFSA because they are more competitive in terms of sheet resistance than the others.

Table 4-1. Sheet resistance achieved by various dopants, as reported in literature.

Dopant	Sheet Resistance (Ohm/sq)
$AuCl_3$	112[28]
HNO_3	125[6]
TFSA	129[25]
$SOCl_2$	405[27]
(F4)TCNQ	1100 for 1L, 100 for 4L[29]
TCNQ	140 for 4L[30]

The doping conditions are as follows. These conditions are reported in literature or obtained through correspondence and have presumably been optimized.

$AuCl_3$ – Dissolve in Nitromethane (10mM) and spin-cast at 2500rpm

HNO3 – Hold graphene sample ~1cm above 70% HNO_3 vapor for 1min

TFSA – Dissolve in Nitromethane (20mM) and spin-cast at 2500rpm

4.2 Points of Comparison

4.2.1   Sheet Resistance and Carrier Concentration

In terms of sheet resistance achieved for monolayer graphene, $FeCl_3$ holds a clear advantage over HNO_3 and TFSA and has a slight advantage over $AuCl_3$. $FeCl_3$ also scales better with increasing layer number than HNO_3 or TFSA. The sheet resistance and carrier concentration versus number of layers are shown in Figure 4-1 and Figure 4-2 respectively. All samples have been acetone-treated and annealed.
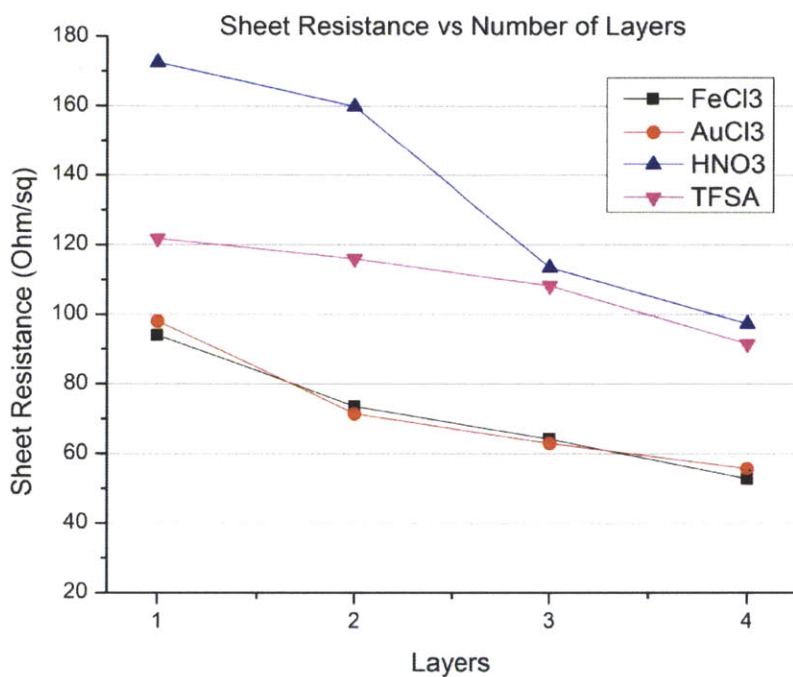

Figure 4-1. Sheet resistance versus layer number for all dopants.
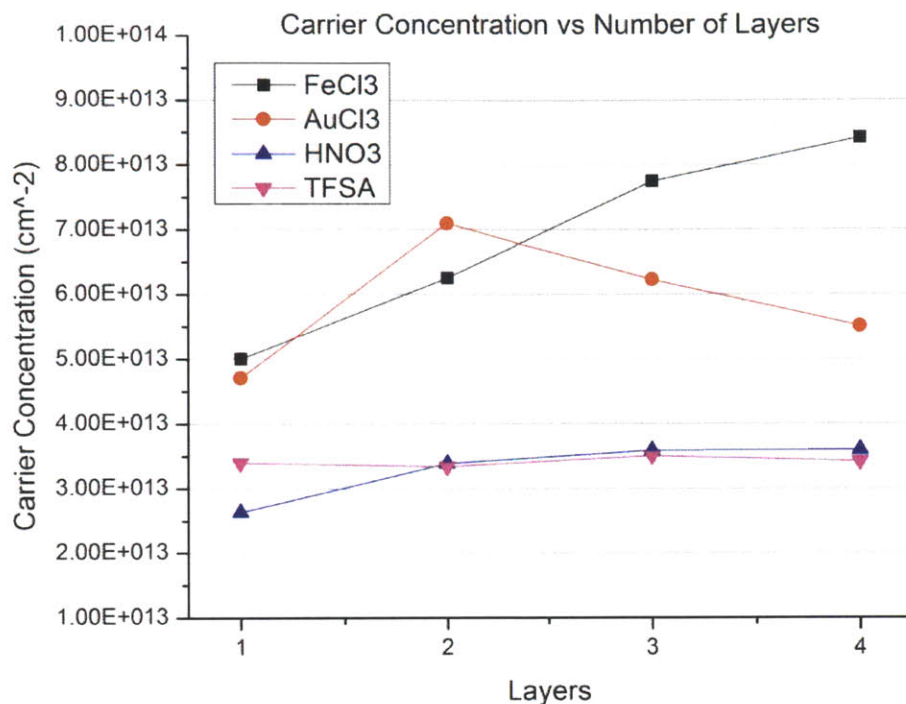
Figure 4-2. Carrier concentration versus layer number for all dopants.

The biggest advantage of $FeCl_3$ with regards to electrical properties is that the carrier concentration continues to increase when more layers are added, even though doping is only done when all layers have been transferred. This is likely because of the differences in doping method. $FeCl_3$ is evaporated at high temperatures, which may allow the dopant to diffuse between the layers in its gaseous state. $AuCl_3$ and TFSA are spin-cast, which only allows the molecules to attach to the topmost layer. HNO_3 doping is a low temperature process so the dopant, again, may only be able to attach to the topmost layer.

We can also infer from our data that the charge transfer effect does not penetrate multiple layers of graphene. Otherwise, the other dopants, like $FeCl_3$, should also be able to continue increasing carrier concentration as more layers are added even though they only sit on the topmost layer.

Another curious trend is that the carrier concentration for $AuCl_3$ starts to decrease when there are more than two layers of graphene. We will reserve the discussion for the section regarding acetone versus annealing.

29

4.2.2 *Stability in Atmosphere*

We compare the sheet resistance and carrier concentration over time for the various dopants. TFSA is reported to be air-stable while $AuCl_3$ and HNO_3 have been shown to be unstable in air. The data is shown below.
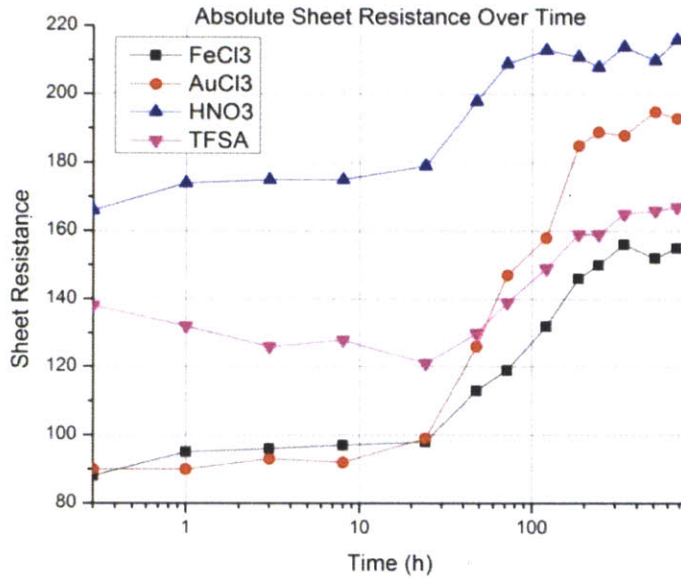

Figure 4-3. Absolute sheet resistance for all dopants over time.
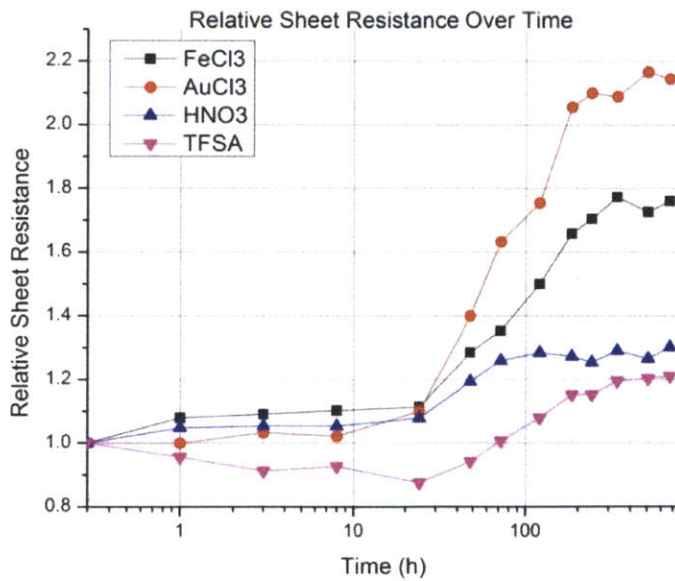

Figure 4-4. Relative sheet resistance for all dopants over time (normalized to initial value).
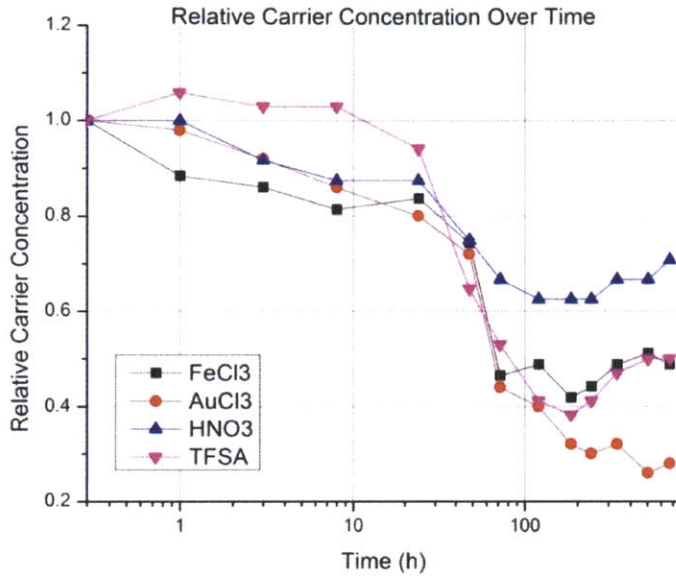
30

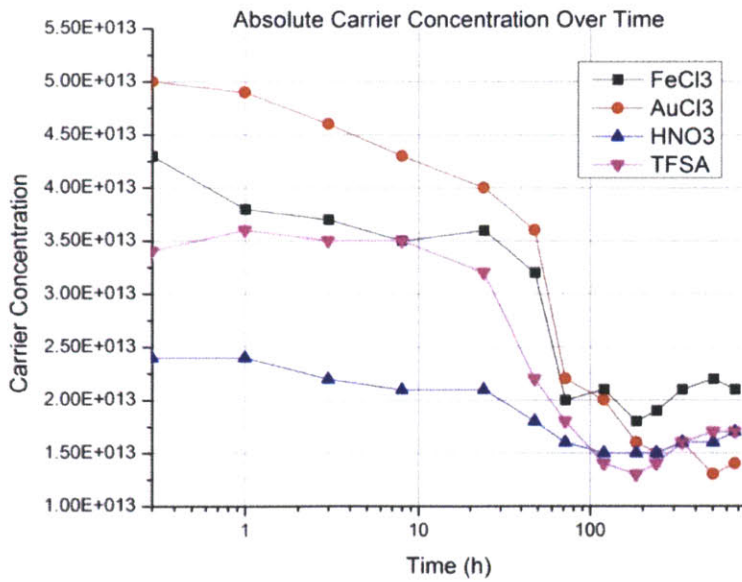Figure 4-5. Absolute carrier concentration for all dopants over time.

Figure 4-6. Relative carrier concentration for all dopants over time (normalized to initial value).

31

In terms of sheet resistance over time, $FeCl_3$ is superior to $AuCl_3$ in air stability but inferior to TFSA and HNO_3. For all dopants, the carrier concentration decreases sharply over the course of 1 week, eventually settling to roughly $1.5 \times 10^{13} cm^{-2}$ after two weeks. The more heavily doped samples ($FeCl_3$, $AuCl_3$) exhibit larger drops than the lighter doped ones (HNO_3). TFSA is an interesting case because even though the carrier concentration drops significantly, the sheet resistance only increases by ~20% because the mobility recovers over time. This would suggest that TFSA damages the samples less than the other dopants. It has been reported that TFSA is completely stable in air for more than 2 weeks but our experiments seem to indicate otherwise[25]. This could be because of different ambient conditions. Nonetheless, TFSA still appears to have the best air stability of all the dopants we discuss. HNO_3 also appears to have reasonably good air stability in spite of other reports in literature but this could be due to the worse starting value. We do note, however, that spin-casting a 300nm layer of PMMA on $FeCl_3$ prevents the conductivity from degrading over time. This is not possible for TFSA because it dissolves in Anisole.

As before, we compare the time evolution of sheet resistance at $130^{\circ}C$ over 120min. Again, the samples are left in air for 24h to separate the effects of initial increase in resistance with time and with temperature.
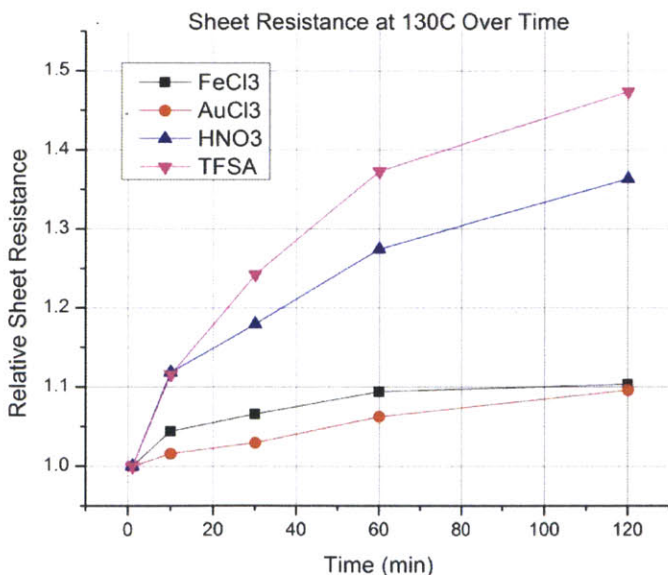
Figure 4-7. Time evolution of sheet resistance for all dopants at 130C.

It would appear that $FeCl_3$ and $AuCl_3$ are quite stable at $130^{\circ}C$ but HNO_3 and TFSA are not; this is most likely due to the different physical properties of the dopants. Both HNO_3 and TFSA are quite volatile at room temperature so it is likely that they would degas quickly at $130^{\circ}C$. $FeCl_3$ and $AuCl_3$ are stable powders at room temperatures and have relatively high boiling points so they would be less prone to evaporation at higher temperatures.

4.2.3 Stability in Solvents

We compare the relative solvent stability of the dopants by immersing for 2min. We use the percentage change in resistance as the primary metric to account for the different starting points.

Table 4-2. Percentage increase in sheet resistance.

	FeCl₃	AuCl₃	HNO₃	TFSA
Water	**182**	Broken	Broken	103
IPA	6	30	7	356
Acetone	63	419	561	Broken
Nitromethane	50	379	117	160
Anisole	3	**40**	5	52

	Small Change (<10%)
	Moderate Change (10-100%)
	Large Change (>100%)
	Sample Discontinuous
bold	*Sample Damaged*

In two cases, FeCl₃ in water and AuCl₃ in Anisole (bolded in Table 4-2), the increase in sheet resistance is substantially larger than the change in carrier concentration. Thus, we can attribute this to degraded mobility, which suggests that the sample was damaged. In other cases, the damage was severe enough that the sample was no longer continuous over a large area and thus did not have measurable sheet resistance. The results are summarized in Figure 4-8.

Table 4-3. Percentage change in carrier concentration.

	FeCl₃	AuCl₃	HNO₃	TFSA
Water	**-36**	Broken	Broken	-66
IPA	-7	-41	-7	-85
Acetone	-38	-83	-91	Broken
Nitromethane	-42	-92	-65	-73
Anisole	-7	**1**	-8	-21
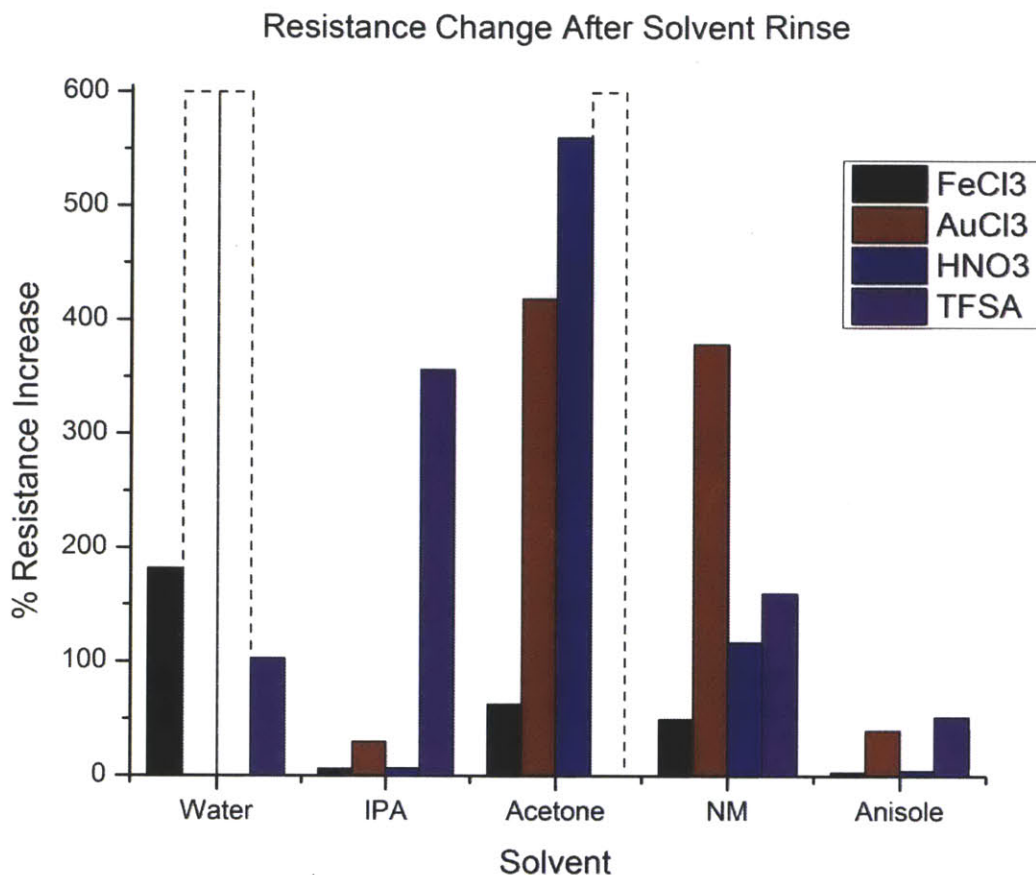
Figure 4-8. Percent change in resistance. Broken samples are shown with dotted lines.

FeCl₃ appears to hold a large advantage over other dopants when it comes to solvent stability; it is very stable in both IPA and Anisole. This allows for the sample to be rinsed after doping if further cleaning is needed and for a PMMA layer to be spin-cast to protect the dopant from oxygen and moisture in air. HNO₃ is also stable in IPA and Anisole, but less stable than FeCl₃ in Acetone and Nitromethane. AuCl₃ and TFSA can be rinsed away or destroyed entirely by any solvent. It is worth noting that all forms of doping studied in this work, including FeCl₃, cannot resist Water, Acetone, or Nitromethane.

4.2.4   Other Considerations

We noted in Chapter 3 that FeCl₃ doping is equally effective for both acetone-treated and annealed samples. The same is not true of AuCl₃, HNO₃, or TFSA.

AuCl$_3$, HNO$_3$, and TFSA are all significantly less effective in reducing sheet resistance for samples that have not been annealed, as shown in Figure 4-9.

Figure 4-9. Sheet resistance and carrier concentration comparison for acetone treatment and annealing.
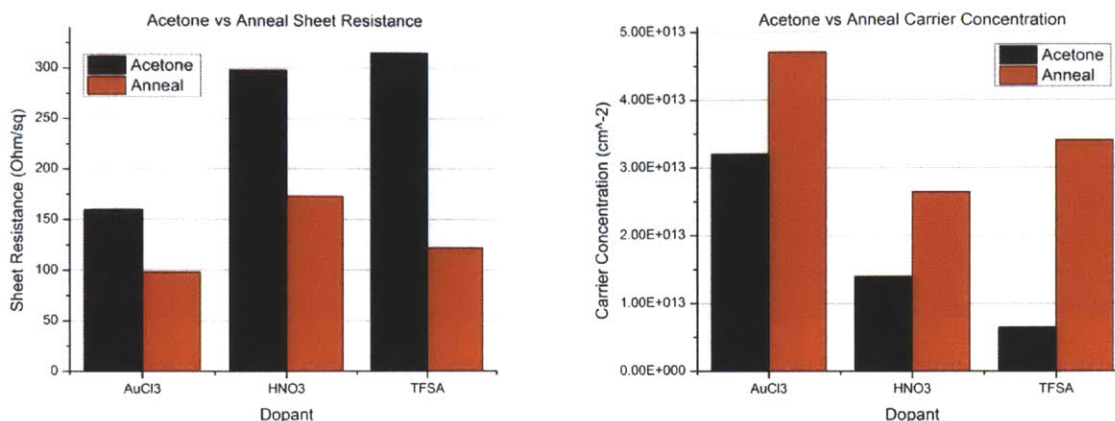
We infer that this is due to mechanical changes in the surface of graphene. It has been shown that graphene conforms more closely to the SiO$_2$ surface after thermal annealing, resulting in a rougher surface profile[31]. This contact with SiO$_2$, combined with exposure to oxygen and moisture in air, causes the carrier concentration to increase to roughly 10^{13}cm^{-2}. Ryu et al. hypothesize that this is because oxygen molecules are stabilized by water and electrostatically bind to the SiO$_2$ surface; the substrate is a critical component in this equation. Thus, it is reasonable to suggest that the same effect may apply to HNO$_3$. Another distinct possibility is that the rougher surface allows AuCl$_3$ and TFSA (which are spin-cast) to wet better.

In this context, we can try to surmise why AuCl$_3$ dopes 3-layer samples less heavily than 2-layer ones. When there are multiple layers of graphene, the bottom layers may shield the top layers from the substrate conforming effect. Furthermore, if AuCl$_3$, like oxygen requires substrate interaction to dope graphene, having additional layers will certainly mitigate the effect. It is not clear how the dopants are fundamentally different. At this point, the explanation is pure conjecture based on previous reports and our limited observations. Further characterization needs to be done to confirm our hypotheses.

Furthermore, in the case of AuCl$_3$, the spin-coating leaves thick layers of residues on samples that have not been annealed, as shown in Figure 4-10. We suspect this may be related to presence of PMMA residues on the graphene after acetone treatment, which may act as nucleation centers for the formation of the bright spots. Again, this is purely conjectural, but we do not investigate this further as AuCl$_3$ doping is not the focus of this work.
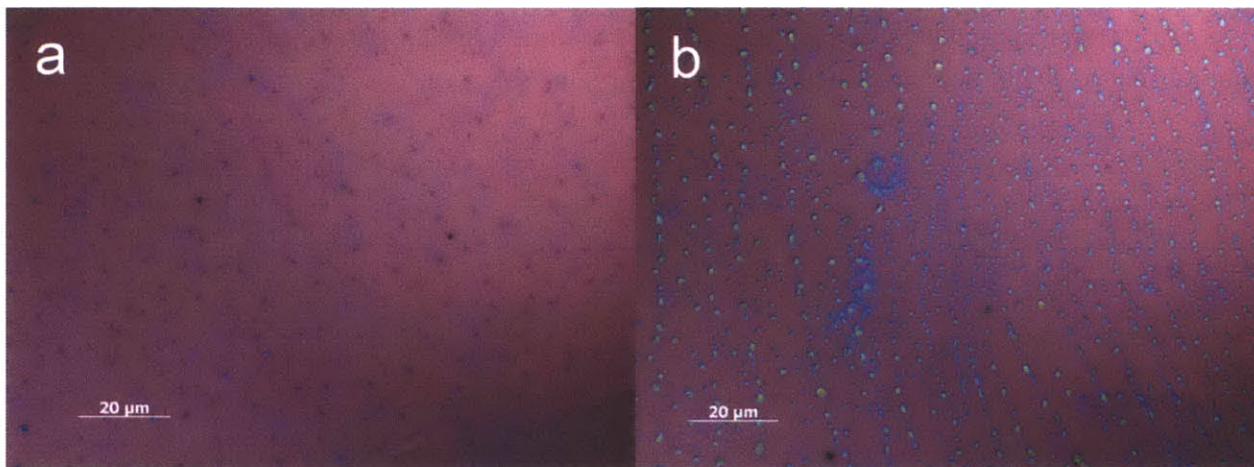
Figure 4-10. Optical images of AuCl$_3$ doped graphene. a) Annealed sample. b) Acetone-treated sample. The bright particles present on the acetone-treated graphene cause the surface of the graphene to appear dull by eye.

Another important consideration is the speed and cost of doping. This is one aspect in which FeCl$_3$ is markedly inferior to its competitors. AuCl$_3$ and TFSA only require a spin coater and HNO$_3$ only requires a petri dish whereas FeCl$_3$ requires a furnace, sealable chamber, and gas flow. Although the actual doping time is short, the overhead time is quite long, as the furnace takes time to heat and the chamber must be washed after several cycles. Scaling is possible, but may be expensive, as the chamber and furnace must encapsulate all samples. Thus, only in certain situations would the advantages of FeCl$_3$ merit the increase in cost and complexity.

Chapter 5

5 Summary and Conclusions

In summary, we have investigated and characterized the doping of CVD graphene using Iron(III) Chloride . We were able to demonstrate that $FeCl_3$ can dope graphene to sheet resistances as low as 72Ohm, which is the best value reported in literature thus far.

Ultimately, the purpose of doping is to increase the carrier concentration, thereby shifting the Fermi level and reducing sheet resistance. All four dopants studied in this work – $FeCl_3$, $AuCl_3$, HNO_3, and TFSA – do this sufficiently well. The difference in sheet resistance achievable by $FeCl_3$ compared to the other dopants is, at first glance, minor and irrelevant, as it is difficult to imagine a device that would work with 95Ohm graphene but would not work with 120Ohm graphene. However, if in the future graphene becomes relevant in industry, performance improvements of 10-20% as a result of higher conductivity would be tremendous.

In terms of relevance to research applications, the main advantage of $FeCl_3$-doped graphene is not achieving lower sheet resistance, but rather, better compatibility with other processes. The key positive points of FeCl3 doping, not necessarily relative to other dopants, can be summarized as follows:

1) All dopants experience diminishing returns with regard to conductivity as the number of graphene layers is increased, but it is not as severe in the case of $FeCl_3$ (and $AuCl_3$).
2) It is stable in some solvents such as IPA and Anisole likely owing to its inorganic nature. This allows a layer of PMMA to be used as a protective coating to prevent degradation over time.
3) It is equally effective for acetone-treated and annealed samples.
4) The doping process is scalable.

However, the negative points are:

1) The doping process is more involved and more difficult to control.
2) The doping process requires high temperatures, albeit for a short period of time, making it impractical for some substrates.
3) Like other dopants, it is not stable in air.
4) Rinsing with water after doping causes the graphene to break.

At the very least, $FeCl_3$ doping is a viable alternative to $AuCl_3$ or HNO_3 and may be superior for some purposes. Because circumstances encountered during research can vary greatly, it is highly advantageous to have a larger repertoire of techniques. Our work thoroughly characterizes this doping method and provides a foundation for applications in the future.

37

References

1. Li, X.; Cai, W.; An, J.; Kim, S.; Nah, J.; Yang, D.; Piner, R.; Velamakanni, A.; Jung, I.; Tutuc, E.; Banerjee, S. K.; Colombo, L.; Ruoff, R. S. *Science* **2009**, 324, (5932), 1312-4.
2. Park, H.; Brown, P. R.; Bulović, V.; Kong, J. *Nano Letters* **2011**, 12, (1), 133-140.
3. Park, H.; Howden, R. M.; Barr, M. C.; Bulović, V.; Gleason, K.; Kong, J. *ACS Nano* **2012**, 6, (7), 6370-6377.
4. Kasry, A.; Kuroda, M. A.; Martyna, G. J.; Tulevski, G. S.; Bol, A. A. *ACS Nano* **2010**, 4, (7), 3839-3844.
5. Tianhua, Y.; Liang, C.-W.; Kim, C.; Eui-Sang, S.; Bin, Y. *Electron Device Letters, IEEE* **2011**, 32, (8), 1110-1112.
6. Bae, S.; Kim, H.; Lee, Y.; Xu, X.; Park, J.-S.; Zheng, Y.; Balakrishnan, J.; Lei, T.; Ri Kim, H.; Song, Y. I.; Kim, Y.-J.; Kim, K. S.; Ozyilmaz, B.; Ahn, J.-H.; Hong, B. H.; Iijima, S. *Nat Nano* **2010**, 5, (8), 574-578.
7. Kim, K. K.; Reina, A.; Shi, Y.; Park, H.; Li, L.-J.; Lee, Y. H.; Kong, J. *Nanotechnology* **2010**, 21, (28), 285205.
8. Yan, C.; Kim, K.-S.; Lee, S.-K.; Bae, S.-H.; Hong, B. H.; Kim, J.-H.; Lee, H.-J.; Ahn, J.-H. *ACS Nano* **2011**, 6, (3), 2096-2103.
9. Ni, G.-X.; Zheng, Y.; Bae, S.; Tan, C. Y.; Kahya, O.; Wu, J.; Hong, B. H.; Yao, K.; Özyilmaz, B. *ACS Nano* **2012**, 6, (5), 3935-3942.
10. Khrapach, I.; Withers, F.; Bointon, T. H.; Polyushkin, D. K.; Barnes, W. L.; Russo, S.; Craciun, M. F. *Advanced Materials* **2012**, 24, (21), 2844-2849.
11. Chen, J.-H.; Jang, C.; Xiao, S.; Ishigami, M.; Fuhrer, M. S. *Nat Nano* **2008**, 3, (4), 206-209.
12. Li, X.; Cai, W.; An, J.; Kim, S.; Nah, J.; Yang, D.; Piner, R.; Velamakanni, A.; Jung, I.; Tutuc, E.; Banerjee, S. K.; Colombo, L.; Ruoff, R. S. *Science* **2009**, 324, (5932), 1312-1314.
13. Reina, A.; Jia, X.; Ho, J.; Nezich, D.; Son, H.; Bulovic, V.; Dresselhaus, M. S.; Kong*, J. *Nano Letters* **2009**, 9, (8), 3087-3087.
14. Cheng, Z. G.; Zhou, Q. Y.; Wang, C. X.; Li, Q. A.; Wang, C.; Fang, Y. *Nano Letters* **2011**, 11, (2), 767-771.
15. Cheng, Z.; Zhou, Q.; Wang, C.; Li, Q.; Wang, C.; Fang, Y. *Nano Letters* **2011**, 11, (2), 767-771.
16. Goossens, A. M.; Calado, V. E.; Barreiro, A.; Watanabe, K.; Taniguchi, T.; Vandersypen, L. M. K. *Appl Phys Lett* **2012**, 100, (7).
17. Lindvall, N.; Kalabukhov, A.; Yurgens, A. *J Appl Phys* **2012**, 111, (6).
18. Suk, J. W.; Lee, W. H.; Lee, J.; Chou, H.; Piner, R. D.; Hao, Y.; Akinwande, D.; Ruoff, R. S. *Nano Letters* **2013**, 13, (4), 1462-1467.
19. Hsu, C.-L.; Lin, C.-T.; Huang, J.-H.; Chu, C.-W.; Wei, K.-H.; Li, L.-J. *ACS Nano* **2012**, 6, (6), 5031-5039.
20. Petrone, N.; Dean, C. R.; Meric, I.; van der Zande, A. M.; Huang, P. Y.; Wang, L.; Muller, D.; Shepard, K. L.; Hone, J. *Nano Letters* **2012**, 12, (6), 2751-2756.
21. Ferrari, A. C.; Meyer, J. C.; Scardaci, V.; Casiraghi, C.; Lazzeri, M.; Mauri, F.; Piscanec, S.; Jiang, D.; Novoselov, K. S.; Roth, S.; Geim, A. K. *Phys Rev Lett* **2006**, 97, (18).
22. Kalbac, M.; Reina-Cecco, A.; Farhat, H.; Kong, J.; Kavan, L.; Dresselhaus, M. S. *ACS Nano* **2010**, 4, (10), 6055-6063.

23. Das, A.; Pisana, S.; Chakraborty, B.; Piscanec, S.; Saha, S. K.; Waghmare, U. V.; Novoselov, K. S.; Krishnamurthy, H. R.; Geim, A. K.; Ferrari, A. C.; Sood, A. K. *Nat Nanotechnol* **2008,** 3, (4), 210-215.

24. Zhao, W. J.; Tan, P. H.; Liu, J.; Ferrari, A. C. *J Am Chem Soc* **2011,** 133, (15), 5941-5946.

25. Tongay, S.; Berke, K.; Lemaitre, M.; Nasrollahi, Z.; Tanner, D. B.; Hebard, A. F.; Appleton, B. R. *Nanotechnology* **2011,** 22, (42).

26. Miao, X.; Tongay, S.; Petterson, M. K.; Berke, K.; Rinzler, A. G.; Appleton, B. R.; Hebard, A. F. *Nano Letters* **2012,** 12, (6), 2745-2750.

27. Li, X. M.; Xie, D.; Park, H.; Zhu, M.; Zeng, T. H.; Wang, K. L.; Wei, J. Q.; Wu, D. H.; Kong, J.; Zhu, H. W. *Nanoscale* **2013,** 5, (5), 1945-1948.

28. Kim, K. K.; Reina, A.; Shi, Y. M.; Park, H.; Li, L. J.; Lee, Y. H.; Kong, J. *Nanotechnology* **2010,** 21, (28).

29. Song, J.; Kam, F.-Y.; Png, R.-Q.; Seah, W.-L.; Zhuo, J.-M.; Lim, G.-K.; Ho, P. K. H.; Chua, L.-L. *Nat Nano* **2013,** advance online publication.

30. Hsu, C. L.; Lin, C. T.; Huang, J. H.; Chu, C. W.; Wei, K. H.; Li, L. J. *ACS Nano* **2012,** 6, (6), 5031-5039.

31. Ryu, S.; Liu, L.; Berciaud, S.; Yu, Y. J.; Liu, H. T.; Kim, P.; Flynn, G. W.; Brus, L. E. *Nano Letters* **2010,** 10, (12), 4944-4951.